Article

Molecule-Based Valence Tautomeric Bistability Synchronized with a Macroscopic Crystal-Melt Phase Transition

Daisuke Kiriya, Ho-Chol Chang, and Susumu Kitagawa

J. Am. Chem. Soc., **2008**, 130 (16), 5515-5522 • DOI: 10.1021/ja711268u • Publication Date (Web): 27 March 2008

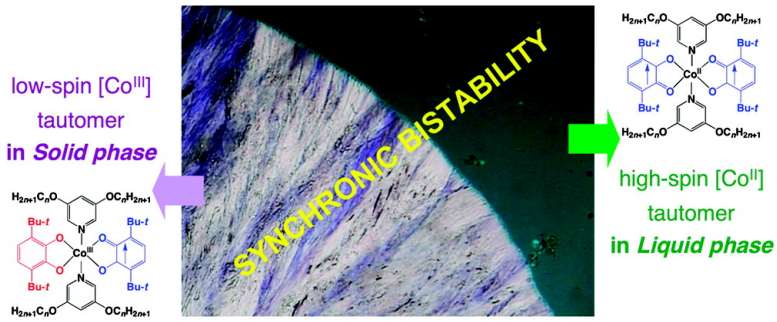

More About This Article

Additional resources and features associated with this article are available within the HTML version:

- Supporting Information
- Access to high resolution figures
- Links to articles and content related to this article
- Copyright permission to reproduce figures and/or text from this article

View the Full Text HTML

J|A|C|S
ARTICLES

Published on Web 03/27/2008

Molecule-Based Valence Tautomeric Bistability Synchronized with a Macroscopic Crystal-Melt Phase Transition

Daisuke Kiriya, Ho-Chol Chang,* and Susumu Kitagawa*

Department of Synthetic Chemistry and Biological Chemistry, Graduate School of Engineering, Kyoto University, Katsura, Nishikyo-ku, Kyoto 615-8510, Japan

Received December 20, 2007; E-mail: chang@sbchem.kyoto-u.ac.jp; kitagawa@sbchem.kyoto-u.ac.jp

Abstract: Here, we show a synchronic bistability of valence tautomeric (VT) molecular interconversion and a macroscopic crystal-melt phase transition in long alkoxy-functionalized cobalt-dioxolene complexes. Studies have been carried out for a novel series of complexes, $[Co(C_nOpy)_2(3,6\text{-DTBQ})_2]$ (3,5-dialkoxy($C_nH_{2n+1}O$-; $n = 9$, 12, and 17)pyridine (C_nOpy) and 3,6-di-*tert*-butyl semiquinonate or catecholate ligands (3,6-DTBQ)). All complexes show the molecular VT interconversion with thermal hysteresis attributed to the synchronous crystal-melt phase transition. Thermodynamic analysis has revealed that the molecular VT interconversion is restricted over 50 K and crystal-melt phase transition is accelerated about 50 K by the synchronicity. The synchronicity is attributed to enthalpic and entropic effects of the alkoxy chains in the crystalline phase of the one tautomer and the melt phase of the other, respectively. Our results show efficient chemical and thermodynamic strategies to combine molecule-based and macroscopic bistabilities.

1. Introduction

The design and synthesis of bistable systems that respond to external stimuli such as heat, light, and magnetic and electric fields are of high scientific and technological significance for high performance devices, including switches, information storage, signal processing, and sensors.[1–7] A great advantage of "molecule-based" bistability lies in its diversity not only in external stimuli that can transform the electronic and/or geometrical states of individual molecules, but also in the interconvertible physical properties.[5,6,8] The central challenges in this field during the past decade have been to introduce cooperative interactions between bistable molecules through supramolecular synthons, particularly in solid phases, providing sharp response, large signal ON/OFF ratio and hysteresis (memory) effects under ambient conditions.[9–13] Although this cooperativity leads to significant improvements in the bistable functionalities derived from the individual molecule, its effects may no longer be limited to molecular scale events, when the molecules communicate strongly with each other. This is because the local structural or electronic changes in a molecule could spread out over a whole region, giving rise to alternative transformations in the spatial orientation and arrangement of other molecules to form energetically favored macroscopic phases. These synergistic effects would appear as macroscopic phase transformations from solid–solid to solid–liquid crystal phase transitions and ultimately a solid–liquid phase transition would be induced. Furthermore, these first-order "phase-based bistabilities"[14–19] allow us to utilize not only the molecular properties of an individual molecule but also integrated properties of molecular assemblies with different morphology, density, volume, fluidity, optic, magnetic, and electric properties to a greater or lesser extent. Thus, a key is to designing molecules that possess internal freedoms both as a molecule and as an

(1) Aviram, A.; Ratner, M. A. *Chem. Phys. Lett.* **1974**, *29*, 277–283.
(2) Feringa, B. L. *Molecular Switches*; Wiley-VCH: Weinheim, Germany, 2001.
(3) Kahn, O.; Launary, J. P. *Chemtronics* **1988**, *3*, 140–151.
(4) Joachim, C.; Gimzewski, J. K.; Aviram, A. *Nature* **2000**, *408*, 541–548.
(5) Irie, M. *Chem. Rev.* **2000**, *100*, 1685–1716.
(6) Balzani, V.; Credi, A.; Raymo, F. M.; Stoddart, J. F. *Angew. Chem., Int. Ed.* **2000**, *39*, 3348–3391.
(7) (a) Beauvais, L. G.; Shores, M. P.; Long, J. R. *J. Am. Chem. Soc.* **2000**, *122*, 2763–2772. (b) Halder, G. J.; Kepert, C. J.; Mouvaraki, B.; Murray, K. S.; Cashion, J. D. *Science* **2002**, *298*, 1762–1765. (c) Maspoch, D.; Ruiz-Molina, D; Wurst, K; Domingo, N; Cavallini, M; Biscarini, F.; Tejada, J.; Rovira, C.; Veciana, J. *Nat. Mater.* **2003**, *2*, 190–195. (d) Ohkoshi, S.; Arai, K.; Sato, Y.; Hashimoto, K. *Nat. Mater.* **2004**, *3*, 857–861.
(8) (a) Dürr, H.; Bouas-Laurent, H. *Photochromism Molecules and Systems*; Elsevier: Amsterdam, The Netherlands, 1990. (b) Kahn, O.; Martinez, C. J. *Science* **1998**, *279*, 44–48. (c) Gütlich, P.; Goodwin, H. A. *Top. Curr. Chem.* **2004**, 233–235. (d) Champin, B.; Mobian, P.; Sauvage, J.-P. *Chem. Soc. Rev.* **2007**, *36*, 358–366. (e) Balzani, V.; Clemente-León, M.; Credi, A.; Ferrer, B.; Venturi, M.; Flood, A. H.; Stoddart, J. F. *Proc. Natl. Acad. Sci. U.S.A.* **2006**, *103*, 1178–1183.
(9) Real, J. A.; Gasper, A. B.; Niel, V.; Muñoz, M. C. *Coord. Chem. Rev.* **2003**, *236*, 121–141.
(10) Collier, C. P.; Mattersteig, G.; Wong, E. W.; Luo, Y.; Beverly, K.; Sampaio, J.; Raymo, F. M.; Stoddart, J. F.; Heath, J. R. *Science* **2000**, *289*, 1172–1175.
(11) Kobatake, S.; Yamada, T.; Uchida, K.; Kato, N.; Irie, M. *J. Am. Chem. Soc.* **1999**, *121*, 2380–2386.
(12) Murray, K. S.; Kepert, C. J. *Top. Curr. Chem.* **2004**, *233*, 195–228.
(13) Itkis, M., E.; Chi, X.; Cordes, A. W.; Haddon, R. C. *Science* **2002**, *296*, 1443–1445.
(14) Braga, D.; Grepioni, F. *Chem. Soc. Rev.* **2000**, *29*, 229–238.
(15) Bernstein, J.; Davery, R. J.; Henck, J. O. *Angew. Chem., Int. Ed.* **1999**, *38*, 3440–3461.
(16) Fujita, W.; Awaga, K. *Science* **1999**, *286*, 261–262.
(17) Brownridge, S.; Du, H.; Fairhurst, S. A.; Haddon, R. C.; Oberhammer, H.; Parsons, S.; Passmore, J.; Schriver, M. J.; Sutcliffe, L. H.; Westwood, N. P. C. *J. Chem. Soc., Dalton Trans.* **2000**, 3365–3382.
(18) McMillan, P. F. *J. Mater. Chem.* **2004**, *14*, 1506–1512.
(19) Demus, D.; Goodby, J.; Gray, G. W.; Spiess, H. W. *Handbook of Liquid Crystals: Fundamentals*; Wiley-VCH: Weinheim, Germany, 1998; Vol. 1.

assembly, and to finding synchronic effects resulting from sufficient correlation between a molecular state and a macroscopic phase. However, recent related studies have not achieved any synchronic bistability[20–25] or have shown only partial synchronicity in solid phases[26–28] or in low-dimensional materials.[29,30] This is because intramolecular electronic energies are at much higher levels than intermolecular potential energies, resulting in a very small influence on the molecular state by macroscopic phase transformations and vice versa.

To achieve efficient correlation between the molecular state and the macroscopic phase, the following two features seem to be important. First, the properties of an individual molecule must play an essential role in the stability of the phase in which the molecule exists. This is because that to cause a drastic macroscopic change, the molecule-based bistability must result in significant perturbation in the intermolecular interactions by changing, for instance, the molecule's permanent dipole moment. The second important feature is that the internal freedoms in intermolecular interactions must be rich to allow formation of two or more assembled phases that can easily be distinguished macroscopically. The consideration of these two features leads us to design and use a valence tautomeric molecule[31–34] functionalized with long alkoxy chains as structural flexible parts. Valence tautomerism (VT) has been known as a representative molecule-based bistability that involves a reversible intramolecular electron transfer within two tautomers that differ in charge distribution under equilibrium conditions.[31–34] In particular, a family of cobalt−dioxolene complexes with the formula $[Co^{III}(L)_2(DTBSQ)(DTBCat)]$ undergoes the reversible VT interconversion represented in Scheme 1, where $DTBSQ^{\cdot-}$ and $DTBCat^{2-}$ refer to monoanionic 3,6-di-*tert*-butyl-semiquinonate and a dianionic 3,6-di-*tert*-butyl-catecholate forms, respectively, and L is a nitrogen-containing auxiliary ligand.[31–35] The first example of this facilitating phenomenon was found by Pierpont and co-workers,[31,32,36] and extensive research has been done by Hendrickson[25,36b,37] and other groups.[33,38] These pioneering works have revealed the mechanism of VT interconversion and also developed the molecular design toward a fine-tuning of molecular bistability. The most prominent feature of VT interconversion is that the two tautomers are related by an intramolecular "single-electron transfer" between DTBCat and the Co^{III} ion as well as a spin change from a low-spin Co^{III} form (ls-[Co^{III}], $S = {}^1/_2$) to a high-spin Co^{II} form (hs-[Co^{II}], $S = {}^3/_2$ with two $S = {}^1/_2$). The VT interconversion is thus entropically driven, giving rise to a large change in magnetic and optical properties through the endothermic (ls-[Co^{III}]-to-hs-[Co^{II}]) and exothermic (hs-[Co^{II}]-to-ls-[Co^{III}])) electron transfer processes.[32,39] Herein we report the first synthesis of VT complexes containing alkoxy chains, [Co(C*n*Opy)$_2$(3,6-DTBQ)$_2$] (Scheme 1, **CoC*n*Opy** = 3,5-dialkoxy($C_nH_{2n+1}O$-; n = 9, 12, and 17)pyridine (C*n*Opy), 3,6-di-*tert*-butyl semiquinonate or catecholate ligands (3,6-DTBQ)), which exhibit a molecular VT interconversion synchronized with a macroscopic phase transition.

Scheme 1. The valence tautomeric bistability in **CoC*n*Opy** (n = 9, 12, and 17) with schematic diagrams of the molecular orbitals.

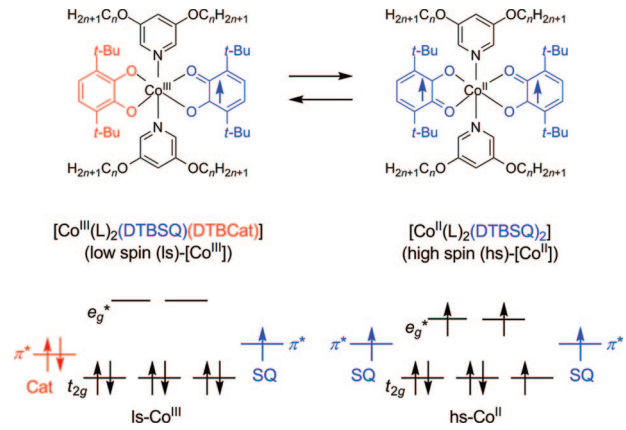

2. Experimental Section

2.1. Materials. Sodium hydride (NaH, Wako), 3,5-dichloropyridine (Tokyo Chemical Industry Co., TCI), 1-nonanol (Aldrich), 1-dodecanol (Wako), and 1-heptanol (TCI) were used without further purification. The starting material [Co(3,6-DTBSQ)$_3$] was prepared by the published procedure.[40]

2.2. Synthesis of 3,5-Dialkoxypyridine.[41] To an anhydrous 75 mL dimethylformamide suspension of NaH (60–72% in oil) (1.5

(20) Aprahamian, I.; Yasuda, T.; Ikeda, T.; Saha, S.; Dichtel, W. R.; Isoda, K.; Kato, T.; Stoddart, J. F. *Angew. Chem., Int. Ed.* **2007**, *46*, 4675–4679.
(21) Baranoff, E. D.; Voignier, J.; Yasuda, T.; Heitz, V.; Sauvage, J.-P.; Kato, T. *Angew. Chem., Int. Ed.* **2007**, *46*, 4680–4683.
(22) Galyametdinov, Y.; Ksenofontov, V.; Prosvirin, A.; Ovchinnikov, I.; Ivanova, G.; Gütlich, P.; Haase, W. *Angew. Chem., Int. Ed.* **2001**, *40*, 4269–4271.
(23) Seredyuk, M.; Gaspar, A. B.; Ksenofontov, V.; Reiman, S.; Galyametdinov, Y.; Haase, W.; Rentschler, E.; Gütlich, P. *Chem. Mater.* **2006**, *18*, 2513–2519.
(24) Hayami, S.; Danjobara, K.; Inoue, K.; Ogawa, Y.; Matsumoto, N.; Maeda, Y. *Adv. Mater.* **2004**, *16*, 869–872.
(25) Adams, D. M.; Dei, A.; Rheingold, A. L.; Hendrickson, D. N. *J. Am. Chem. Soc.* **1993**, *115*, 8221–8229.
(26) Kiriya, D.; Chang, H.-C.; Kitagawa, S. *Dalton Trans.* **2006**, 1377–1382.
(27) Kobatake, S.; Takami, S.; Muto, H.; Ishikawa, T.; Irie, M. *Nature* **2007**, *446*, 778–781.
(28) Hayami, S.; Moriyama, R.; Shuto, A.; Maeda, Y.; Ohta, K.; Inoue, K. *Inorg. Chem.* **2007**, *46*, 7692–7694.
(29) Ikeda, T.; Mamiya, J.; Yanlei, Y. *Angew. Chem., Int. Ed.* **2007**, *46*, 506–528.
(30) Fujigaya, T.; Jiang, D.-L.; Aida, T. *J. Am. Chem. Soc.* **2003**, *125*, 14690–14691.
(31) Buchanan, R. M.; Pierpont, C. G. *J. Am. Chem. Soc.* **1980**, *102*, 4951–4957.
(32) Pierpont, C. G. *Coord. Chem. Rev.* **2001**, *216–217*, 99–125.
(33) Gütlich, P.; Dei, A. *Angew. Chem., Int. Ed.* **1997**, *36*, 2734–2736.
(34) Pierpont C. G.; Kitagawa, S. *Inorganic Chromotropism*; Kodansha/Springer: Tokyo, 2007; pp 116−142.
(35) Attia, A. S.; Jung, O.-S.; Pierpont, C. G. *Inorg. Chim. Acta* **1994**, *226*, 91–98.
(36) (a) Pierpont, C. G.; Buchanan, R. M. *Coord. Chem. Rev.* **1981**, *38*, 45–87. (b) Hendrickson, D. N.; Pierpont, C. G. *Top. Curr. Chem.* **2004**, *234*, 63–95.
(37) (a) Roux, C.; Adams, D. M.; Itié, J. P.; Polian, A.; Hendrickson, D. N.; Verdaguer, M. *Inorg. Chem.* **1996**, *35*, 2846–2852. (b) Adams, D. M.; Li, B. L.; Hendrickson, D. N. *Angew. Chem., Int. Ed.* **1995**, *34*, 1481–1483.
(38) (a) Abakumov, G. A.; Cherkasov, V. K.; Bubnov, M. P.; Éllert, O. G.; Dobrokhotova, Zh. B.; Zakharov, L. N.; Struchkov, Yu. T. *Dokl. Akad. Nauk* **1993**, *328*, 332–335. (b) Shultz, D. A. *Magnetism: Molecules to Materials II*; Wiley-VCH: Weinheim, Germany, 2001; pp 281−306. (c) Dei, A.; Gatteschi, D.; Sangregorio, C.; Sorace, L. *Acc. Chem. Res.* **2004**, *37*, 827−835. (d) Evangelio, E.; Ruiz-Molina, D. *Eur. J. Inorg. Chem.* **2005**, 2957–2971. (e) Sato, O.; Cui, J. A.; Matsuda, R.; Tao, J.; Hayami, S. *Acc. Chem. Res.* **2007**, *40*, 361–369.
(39) Pierpont, C. G.; Jung, O.-S. *Inorg. Chem.* **1995**, *34*, 4281–4282.
(40) Lange, C. W.; Conklin, B. J.; Pierpont, C. G. *Inorg. Chem.* **1994**, *33*, 1276–1283.
(41) Testaferri, L.; Tingoli, M.; Bartoli, D.; Massoli, A. *Tetrahedron* **1985**, *41*, 1373–1384.

Table 1. Crystallographic Data and Structure Refinement Parameters for **CoC*n*Opy** (n = 9, 12, and 17)

	CoC9Opy	CoC12Opy	CoC17Opy
formula	$C_{74}H_{122}CoN_2O_8$	$C_{86}H_{146}CoN_2O_8$	$C_{106}H_{186}CoN_2O_8$
formula weight	1226.67	1394.98	1675.50
crystal system	triclinic	triclinic	triclinic
space group	$P\bar{1}$	$P\bar{1}$	$P\bar{1}$
a (Å)	10.370(4)	10.3238(19)	10.239(5)
b (Å)	11.147(5)	11.0821(19)	11.233(7)
c (Å)	16.958(6)	20.529(3)	23.234(13)
α (deg)	81.84(2)	72.571(7)	85.803(13)
β (deg)	71.978(16)	75.310(9)	77.468(15)
γ (deg)	86.48(2)	85.763(10)	86.421(13)
V (Å^3)	1844.8(12)	2167.7(6)	2599(2)
density (g/cm^3)	1.104	1.069	1.071
Z	1	1	1
T (K)	213(2)	213(2)	213(2)
μ (mm^{-1})	0.284	0.249	0.217
$R1$ [$I > 2\sigma(I)$] [a]	0.0564	0.0569	0.0648
$wR2$ [$I > 2\sigma(I)$][b]	0.1554	0.1546	0.1679
GOF	1.064	1.050	1.045

[a] $R1 = \Sigma||F_o| - |F_c||/\Sigma|F_o|$. [b] $wR2 = [\Sigma w(F_o^2 - F_c^2)^2/\Sigma w(F_o^2)^2]^{1/2}$.

g, 40 mmol) in a 300 mL three-neck flask equipped with a magnetic stirrer and a rubber septum, was added $C_nH_{2n+1}OH$ (n = 9, 12, and 17) (40.2 mmol) at 273 K. Gas evolved and the gray suspension was stirred for 140 min at room temperature, and then 3,5-dichloropyridine (0.758 g, 5.12 mmol) was added. On addition of the pyridine a khaki-colored suspension was produced; on further stirring at 358 K for 60 h a bright orange suspension was produced. The reaction was quenched by adding H_2O (100 mL), and the organic material was extracted with CH_2Cl_2 (50 mL × 4). The combined organic layers were washed with water, dried with Na_2SO_4 and $MgSO_4$, and concentrated under reduced pressure to give a brown-yellow liquid.Recrystallization of this liquid from hot, absolute ethanol gave white crystals of the product. 3,5-Dinonyloxypyridine, 21% yield. ^{1}H NMR (500 MHz, $CDCl_3$) δ 0.85–0.88 (t, 6H), 1.26–1.33 (m, 20H), 1.40–1.46 (m, 4H), 1.74–1.79 (m, 4H), 3.95–3.97 (t, 4H), 6.71 (t, 1H), 7.89 (d, 2H). 3,5-Didodecyloxypyridine, 22% yield. ^{1}H NMR (500 MHz, $CDCl_3$) δ 0.84–0.87 (t, 6H), 1.24–1.31 (m, 32H), 1.39–1.45 (m, 4H), 1.73–1.79 (m, 4H), 3.94–3.97 (t, 4H), 6.73–6.74 (t, 1H), 7.89 (d, 2H). 3,5-Diheptadecyloxypyridine, 33% yield. ^{1}H NMR (500 MHz, $CDCl_3$) δ 0.85–0.88 (t, 6H), 1.24–1.31 (m, 52H), 1.39–1.47 (m,4H), 1.71–1.79 (m, 4H), 3.95–3.97 (t, 4H), 6.69–6.70 (t, 1H), 7.89–7.90 (d, 2H).

2.3. Synthesis of [Co(C*n*Opy)$_2$(3,6-DTBQ)$_2$] (CoC*n*Opy, *n* = 9, 12, and 17). A 10 mL toluene suspension containing 0.19 mmol of [Co(3,6-DTBSQ)$_3$] was treated with 0.50 mmol of 3,5-dialkoxy($C_nH_{2n+1}O$-)pyridine (n = 9, 12, and 17) dissolved in a 11 mL of toluene under N_2 atmosphere. The suspension rapidly turned from dark purple to the dark green of the pyridine adduct. The mixture was stirred for 3 h at 353 K, and then acetonitrile was added and the mixture was left at room temperature for several days. Dark violet crystals were obtained after filtration, and then recrystallized from toluene/acetonitrile. [Co(C9Opy)$_2$(3,6-DTBQ)$_2$] (**CoC9Opy**), 47% yield. Anal. Calcd for $C_{74}H_{122}CoN_2O_8$: C, 72.45; H, 10.02; N, 2.28. Found: C, 72.04; H, 9.83; N, 2.36. [Co(C12Opy)$_2$(3,6-DTBQ)$_2$] (**CoC12Opy**), 89% yield. Anal. Calcd for $C_{86}H_{146}CoN_2O_8$: C, 74.04; H, 10.55; N, 2.01. Found: C, 74.29; H, 10.58; N, 2.17. [Co(C17Opy)$_2$(3,6-DTBQ)$_2$] (**CoC17Opy**), 95% yield. Anal. Calcd for $C_{106}H_{186}CoN_2O_8$: C, 75.98; H, 11.19; N, 1.67. Found: C, 75.93; H, 11.05; N, 1.78.

2.4. Physical Measurements. Elemental analysis was performed on a Flash EA 1112 series (Thermo Finnigan instrument). Microscopic analysis was carried out on the samples between two glass slides using a BX51 microscope (Olympus) with an LK-600 hot stage (Linkam) under N_2 atmosphere. Different scanning calorimetric measurements were measured on a DSC 822e (Mettler) under N_2 atmosphere. Variable temperature X-ray diffraction measurements were carried out with Cu Kα radiation equipped with a RINT-2000 diffractometer (Rigaku). Temperature-dependent absorption spectra were recorded on KBr pellets (ca. 0.12 mol %) using a U-3500 spectrophotometer (Hitachi) over the range 185–3200 nm equipped with an Optistat DN cryostat (Oxford Instruments). Magnetic susceptibilities were recorded over the temperature range 5–400 K at 1 T with a superconducting quantum interference device (Quantum Design). All values were corrected for diamagnetism using Pascal's constants.[42] ^{1}H NMR spectroscopy was performed in $CDCl_3$ using an A-500 spectrometer (JEOL), where chemical shifts were determined with respect to $CHCl_3$ (δ = 7.24) as an internal standard.

2.5. X-ray Crystallographic Data. Crystallographic measurements for **CoC9Opy**, **CoC12Opy**, and **CoC17Opy** were performed on a Rigaku mercury diffractometer with a CCD two-dimensional detector with Mo Kα radiation employing a graphite monochromator. Data were collected at 213 K. The sizes of unit cells were estimated from the reflections collected on the setting angles of seven frames (**CoC9Opy** and **CoC12Opy**) and eighteen frames (**CoC17Opy**) by changing ω by 0.5° for each frame. Two or three different χ settings were used, and ω was changed by 0.5° per frame. Intensity data were collected in 991 (**CoC9Opy**), 720 (**CoC12Opy**), and 1440 (**CoC17Opy**) frames (exposure time = 40 (**CoC9Opy**), 30 (**CoC12Opy**), and 30 (**CoC17Opy**) sec/image). Empirical absorption correction using the program REQABA[43] was performed. In all cases, the structures were solved by a direct method (SIR 97)[44] and refined on F^2 in SHELXL-97.[45] The crystallographic data are summarized in Table 1. CCDC-668244 (**CoC9Opy**), CCDC-668245 (**CoC12Opy**), and CCDC-668246 (**CoC17Opy**) contain the supplementary crystallographic data for this paper. These

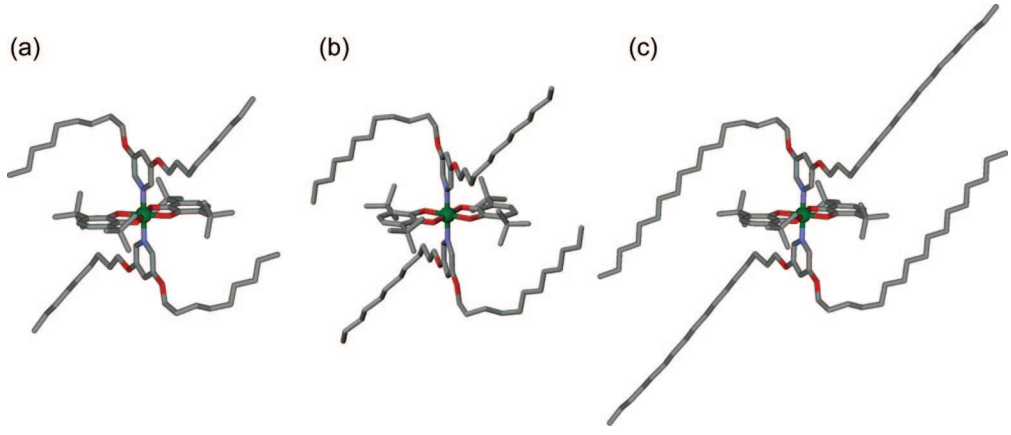

Figure 1. Molecular structures of **CoC*n*Opy** ((a) n = 9, (b) 12, and (c) 17) at 213 K. Color code: green (Co), red (O), blue (N), and grey (C). Hydrogen atoms are omitted for clarity.

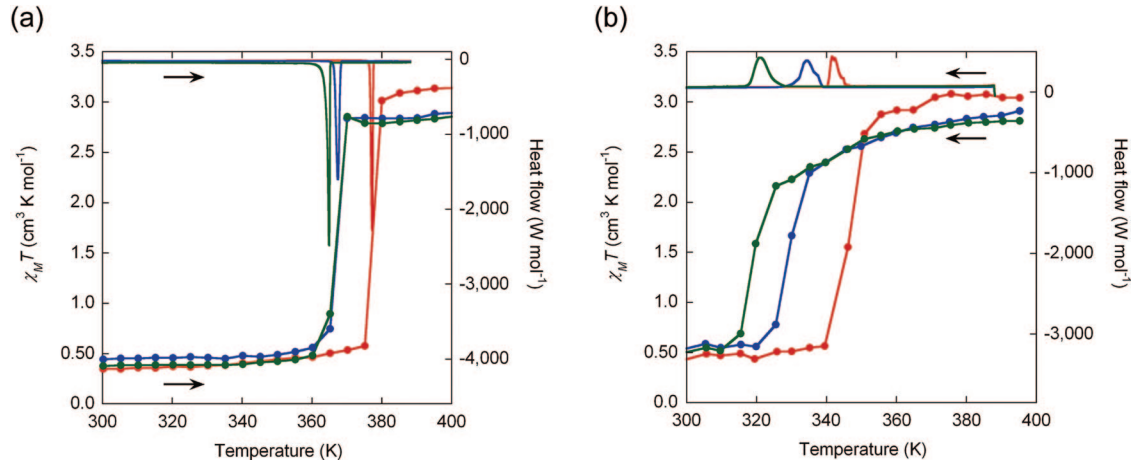

Figure 2. Plots of the temperature dependent magnetic susceptibility (dots with line) and DSC curves (line) observed for **CoC*n*Opy** ($n = 9$ (red), 12 (blue), and 17 (green)) on (a) the first heating and (b) the first cooling processes at a scan rate of 1 K min^{-1}.

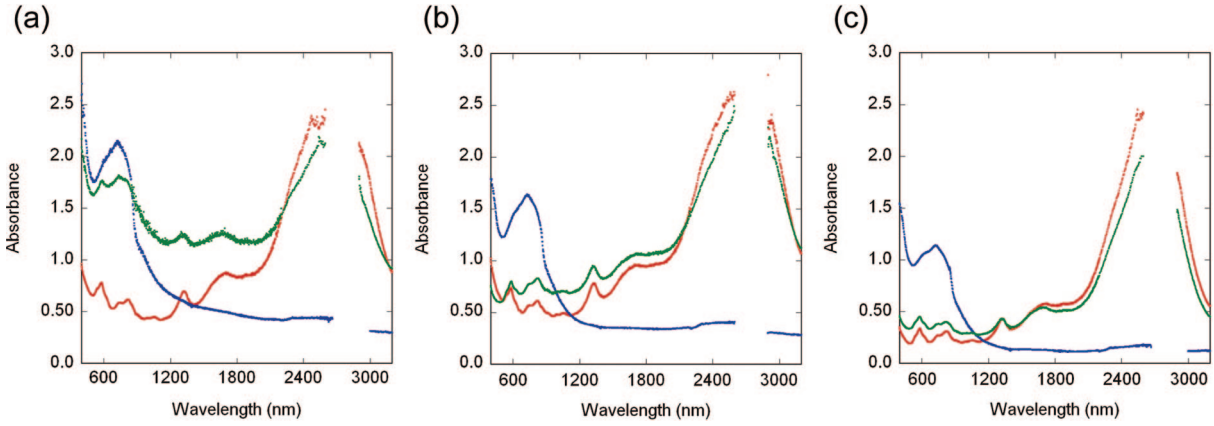

Figure 3. Optical bistability appeared in the temperature-dependent absorption spectra of **CoC*n*Opy** ((a) $n = 9$, (b) 12, and (c) 17) measured on KBr pellets at 300 (red), 400 (blue), and 300 K (green, after cooling from 400 K). The blank region is caused by the optical absorption of the synthetic vitreous silica windows. The absorption maxima of the green line are identical with that of the red line (the virgin sample).[47]

data can be obtained free of charge from The Cambridge Crystallographic Data Center via www.ccdc.cam.ac.uk/data_request/cif.

3. Results and Discussion

A mixture of tris(3,6-di-*tert*-butylsemiquinonate)cobalt(III) and 3,5-dialkoxypyridine (C*n*Opy ($n = 9$, 12, and 17)) in toluene yielded a newly designed [Co(C*n*Opy)$_2$(DTBQ)$_2$] (**CoC*n*Opy**, Scheme 1), where DTBQ indicates either DTBSQ$^{\cdot-}$ or DTBCat^{2-} without charge assignments. The crystal structures of **CoC*n*Opy** at 213 K revealed that the Co atom is located at the crystallographic inversion center that requires a trans coordination geometry and the crystallographically averaged dioxolene ligands (Figure 1). All complexes have the Co−N bond lengths in the region of 1.939(2)–1.950(2) Å and the Co−O bond lengths of 1.864(2)–1.872(1) Å, which are characteristic for an ls-[Co^{III}] form, as reported previously.[25,31,32] The crystals show temperature-independent $\chi_M T$ values characteristic of the $S = {}^1/_2$ spin state in the region of 5–375 (**CoC9Opy**) and 5–360 K (**CoC12Opy** and **CoC17Opy**) as shown in Figure 2a. A strong absorption band around 2500 nm at 300 K (Figure 3) can be assigned to an intramolecular intervalence charge transfer (IVCT) band from the DTBCat^{2-} to the DTBSQ$^{\cdot-}$.[32,46] In addition to the structural parameters, both magnetic and

Table 2. Transition Temperatures ($T_{1/2\uparrow}$, $T_{1/2\downarrow}$, T_m, and T_{cry}), Enthalpy (ΔH_m), and Entropy (ΔS_m) for **CoC*n*Opy** ($n = 9$, 12, and 17) Evaluated from Temperature Dependent Magnetic Sceptibility and DSC Analysis

	CoC9Opy	CoC12Opy	CoC17Opy
$T_{1/2\uparrow}$ (K)[a]	379	367	367
$T_{1/2\downarrow}$ (K)[a]	346	330	319
T_m (K)[b]	377	367	365
T_{cry} (K)[b]	342	334	321
$T_{1/2\uparrow}$ - $T_{1/2\downarrow}$ (K)	33	37	48
ΔH_m (kJ/mol)[c]	80.9	103	130
ΔS_m (J/mol K)[c]	215	281	356

[a] These parameters were determined from the magnetic susceptibility data. [b] These parameters were determined from the DSC analysis. [c] These parameters were determined from the DSC analysis on the first heating process. See the text for the definition of the parameters $T_{1/2\uparrow}$, $T_{1/2\downarrow}$, T_m, and T_{cry}.

(42) Kahn, O. *Molecular Magnetism*; Wiley-VCH: Weinheim, Germany, 1993.
(43) Jacobson, R. A. *REQABA Empirical Absorption Correction,* version 1.1–0310; Molecular Structure Corp.: The Woodlands, TX, 1998.
(44) Altomare, A.; Burla, M. C.; Camalli, M.; Cascarano, G. L.; Giacovazzo, C.; Guagliardi, A.; Moliterni, A. G. G.; Polidori, G.; Spagna, R. *J. Appl. Crystallogr.* **1999**, *32*, 115–119.
(45) Sheldrick, G. M. *SHELXL97*; University of Göttingen: Göttingen, Germany, 1997.
(46) Adams, D. M.; Noodleman, L.; Hendrickson, D. N. *Inorg. Chem.* **1997**, *36*, 3966–3984.

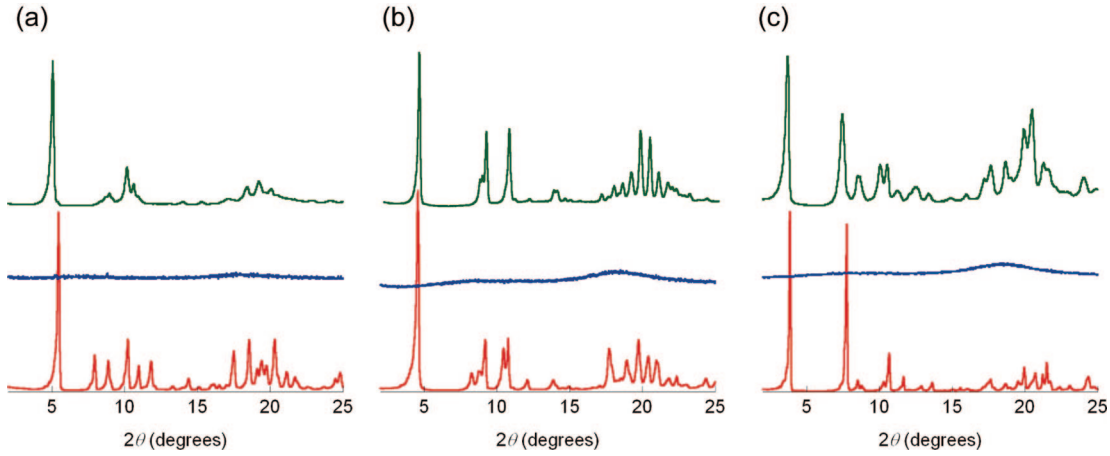

Figure 4. Temperature-dependent X-ray powder diffraction patterns for (a) **CoC9Opy**: the original crystals (bottom, red, 213 K), the melt (middle, blue, 383 K), and the crystals obtained by recrystallization at 353 K for 7 h (top, green, 213 K). (b) **CoC12Opy**: the original crystals (bottom, red, 213 K), the melt (middle, blue, 373 K), and the crystals obtained by recrystallization at a scan rate of 1 K min^{-1} (top, green, 213 K). (c) **CoC17Opy**: the original crystals (bottom, red, 213 K), the melt (middle, blue, 373 K), and the crystals obtained by recrystallization at 328 K for 3 h (top, green, 213 K).[48]

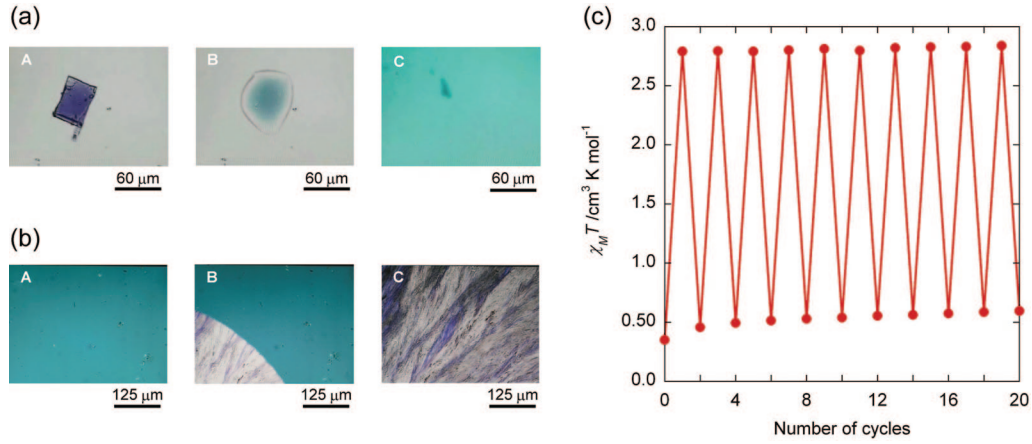

Figure 5. Snapshots of (a) the melting process around 370 K and (b) the crystallization process around 335 K of **CoC12Opy** between two glass slides at a scan rate of 1 K min^{-1}. The green region is the hs-[Co^{II}] tautomer in the melt. The ls-[Co^{III}] tautomer forms the spherulites mutually colored with violet and white around 335 K on the cooling process. (c) The repeated VT interconversion of **CoC12Opy** monitored by the magnetic susceptibility at 300 and 400 K.

spectroscopic features provide a strong indication for the ls-[Co^{III}] form with the mixed-valent ligands in the crystalline phase.

Further temperature-dependent magnetic and optical measurements showed the fundamental features of a molecule-based bistability of **CoC*n*Opy**. On heating the crystals, the magnetic susceptibilities abruptly increased to 3.01 (**CoC9Opy**), 2.84 (**CoC12Opy**), and 2.86 (**CoC17Opy**) cm^3 K mol^{-1} near 380 (**CoC9Opy**) and 370 K (**CoC12Opy** and **CoC17Opy**) (Figure 2a), respectively, and at this temperature the IVCT band characteristic for the ls-[Co^{III}] form disappeared concomitantly (Figure 3). These magnetic and optical changes are attributable to the VT interconversion from the ls-[Co^{III}] form to the hs-[Co^{II}] form (Scheme 1). Differential scanning calorimetric (DSC) studies also revealed that the ls-[Co^{III}] crystals of **CoC*n*Opy** exhibited a sharp endothermic peak at 377 (**CoC9Opy**), 367 (**CoC12Opy**), and 365 K (**CoC17Opy**) (T_m) during the first heating process at a scan rate of 1 K min^{-1} (Figure 2a and Table 2). The magnetic and DSC curves in Figure 2a clearly show that the observed T_m is entirely superimposed on temperature, $T_{1/2t}$, at which the $\chi_M T$ value reaches the average values of the ls-[Co^{III}] and the hs-[Co^{II}] forms. Surprisingly, the thermodynamic parameters ΔH_m and ΔS_m, which were estimated from the DSC study (Table 2), are significantly larger than $\Delta H = 32$ kJ mol^{-1} and $\Delta S = 98$ J K^{-1} mol^{-1}, obtained for the genuine VT complex, [Co(bpy)(3,5-DTBQ)$_2$] (3,5-DTBQ = 3,5-di-*tert*-butyl-semiquinonate or catecholate; bpy = 2,2′-bipyridine),[39] suggesting the presence of additional thermal events.

To shed light on these additional thermal events accompanied by the observed VT interconversion, X-ray diffraction (XRD) experiments were carried out. On heating, a sharp XRD pattern of the virgin crystals of **CoC*n*Opy** (Figure 4, bottom) completely disappears at T_m to give a featureless XRD pattern (Figure 4, middle), undoubtedly demonstrating a crystal-to-melt phase transition. Microphotographs visually demonstrate that the deep violet virgin crystals melt to an optically isotropic green melt with high fluidity (Figure 5a and Supporting Information movie1.mov). In the course of successive cooling of the melt,

(47) The peaks around 550, 800, and 1300 nm at 300 K could be assigned to $\pi-\pi^*$ (Co t_{2g} orbitals to SQ π^* and Cat π^* orbitals), ligand-field transition and LMCT (Cat π^* orbital to Co e_g^* orbitals), and LMCT (Cat π orbital to Co e_g^* orbitals) transition, respectively, while the absorption peak around 700 nm at 400 K could be assigned to a MLCT transition from the Co t_{2g} orbitals to the SQ π^* orbital with the character of ligand-field transition (Co t_{2g} to Co e_g^*).

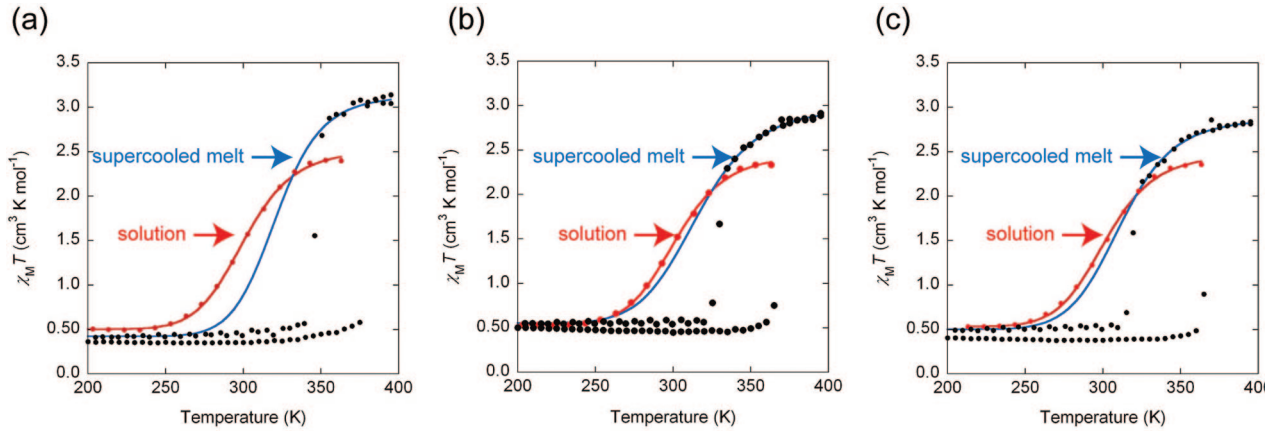

Figure 6. Temperature dependence of $\chi_m T$ of **CoC*n*Opy** ((a) $n = 9$, (b) 12, and (c) 17) in the crystal and the melt (black dots) and in toluene solution (red dots) together with the fitted curves (solid lines).

the $\chi_M T$ value first decreases gradually, and then abruptly drops to the value for the ls-[Co^{III}] form at 346 (**CoC9Opy**), 330 (**CoC12Opy**), and 319 K (**CoC17Opy**) ($T_{1/2\downarrow}$), attending a hysteresis loop of 33 (**CoC9Opy**), 37 (**CoC12Opy**), and 48 K (**CoC17Opy**) (Figure 2b and Table 2).

At the same time, the IVCT band reappears, with the absorption maximum near 2500 nm (Figure 3), indicative of the reverse VT interconversion from the *hs*-[Co^{II}] to the ls-[Co^{III}] form. The DSC studies clearly show that the exothermic peak (T_{cry}) at 342 (**CoC9Opy**), 334 (**CoC12Opy**), and 321 K (**CoC17Opy**) is superimposed on $T_{1/2\downarrow}$, at which $\chi_M T$ values abruptly decrease. Recovery of the original crystalline phase was confirmed by the reappearing XRD pattern (Figure 4, top), which is identical to that of the virgin crystals except for the absence of a few reflections resulting from the oriented crystallization.[48] The microphotographic studies on **CoC12Opy** sandwiched between two glass slides afforded a visual interpretation of the crystallization process, in which highly anisotropic spherulites mutually colored with violet and white gradually begin to grow from the supercooled melt during the cooling at a scan rate of 1 K min^{-1} (Figure 5b and Supporting Information movie2.mov).

As the above results show, the melting and the crystallization processes synchronized perfectly with the ls-[Co^{III}]-to-hs-[Co^{II}] and the hs-[Co^{II}]-to-ls-[Co^{III}] VT interconversions, respectively. These observations can be rephrased as "synchronic bistability", where the molecular states and the macroscopic phases are simultaneously interconverted with inseparable correlation. Consequently, this regime allows us to define one of the two bistable states by means of the properties attributed to the VT tautomers, such as optical and magnetic signals, at one time or from those of macroscopic phases, such as morphology, fluidity, and optical signal, at the other time. This synchronic bistability could be repeated over several cycles and detected by magnetic measurements (Figure 5c), where the $\chi_M T$ values of the two tautomers remain unchanged with sufficient resistance to fatigue during the cycles.

To reveal the mechanism of the observed synchronic bistability, the temperature dependency of $\chi_M T$ of the supercooled melt during the cooling process was studied. The observed temperature dependency of $\chi_M T$ was fitted using least-squares by eq 1[3,49] with an assumption that the melt is in an isolated state with negligible intermolecular interactions (Figure 6).

$$\chi_M T = (\chi T_{hs-[Co^{II}]} - \chi T_{ls-[Co^{III}]})/(1 + \exp\{(\Delta H_{VT(x)} - T\Delta S_{VT(x)})/RT\}) + \chi T_{ls-[Co^{III}]} \quad (1)$$

where $\chi T_{hs\text{-}[Co^{II}]}$ and $\chi T_{ls\text{-}[Co^{III}]}$ represent the limited χT values for the hs-[Co^{II}] and ls-[Co^{III}] forms, respectively, $\Delta H_{VT(x)}$ and

Table 3. Fitting Parameters for the Melt and the Solution of **CoC*n*Opy** ($n = 9$, 12, and 17)

	CoC9Opy	CoC12Opy	CoC17Opy
For the Supercooled Melt			
$\chi T_{ls\text{-}[Co^{III}]}$ (cm^3 K/mol) (melt)[a]	0.42	0.55	0.50
$\chi T_{hs\text{-}[Co^{II}]}$ (cm^3 K/mol) (melt)[b]	3.13	2.97	2.87
R (melt)[b]	0.9998	0.9996	0.9998
$\Delta H_{VT(melt)}$ (kJ/mol)[b]	59.2[f]	43.3	47.3
$\Delta S_{VT(melt)}$ (J/mol K)[b]	184[f]	137	152
$T_{VT(melt)}$ (K)	322	316	311
For the Toluene Solution			
$\chi T_{ls\text{-}[Co^{III}]}$ (cm K/mol) (solution)[a]	0.50	0.53	0.53
$\chi T_{hs\text{-}[Co^{II}]}$ (cm^3 K/mol) (solution)[c]	2.52	2.45	2.47
R (solution)[c]	0.9997	0.9998	0.9996
$\Delta H_{VT\ (solution)}$ (kJ/mol)[c]	47.2	46.5	47.3
$\Delta S_{VT\ (solution)}$ (J/mol K)[c]	157	154	157
$T_{VT(solution)}$ (K)	301	302	301
Thermodynamic Parameters for the Supposed Melting of ls-[Co^{III}] Crystals without VT			
$\Delta H_{m(ls\text{-}[Co^{III}])}$ (kJ/mol)[d]	21.7[f]	59.7	82.7
$\Delta S_{m(ls\text{-}[Co^{III}])}$ (J/mol K)[e]	31.0[f]	144	204
$T_{m(ls\text{-}[Co^{III}])}$ (K)	700[f]	415	405
Thermal Effects of the Synchronicity			
$T_m - T_{VT(melt)}$ (K)	55	51	54
$T_m - T_{m(ls\text{-}[Co^{III}])}$ (K)	−323[f]	−48	−40

[a] These parameters were fixed to the values obtained at 200 (in the melt) and 203 K (in the toluene solution). [b] These parameters were obtained from the fitting curves of the melt. [c] These parameters were obtained from the fitting curves of the temperature dependent magnetic susceptibility in toluene solution obtained by the Evans method. [d] These parameters were obtained from eq 2, using the parameters of $\Delta H_{VT(melt)}$. [e] These parameters were obtained from the eq 3, using the parameters of $\Delta S_{VT(melt)}$. [f] For **CoC9Opy**, the fitting analyses would lead to the overestimated $\Delta H_{VT\ (melt)}$ and $\Delta S_{VT\ (melt)}$ because of a few collected data points for the supercooled melt. This is unavoidable because of the relatively high crystallization nature of **CoC9Opy**. See the text for the definition of the parameters.

(48) The crystallinity becomes lower when the alkyl chain length is shortened. Compounds with shorter alkyl chains tend to require a slower cooling rate or longer aging time to return to the original state. This might be due to kinetically hindered crystal growing processes, which are significantly affected by the cooling rate.

(49) Adams, D. M.; Hendrickson, D. N. *J. Am. Chem. Soc.* **1996**, *118*, 11515–11528.

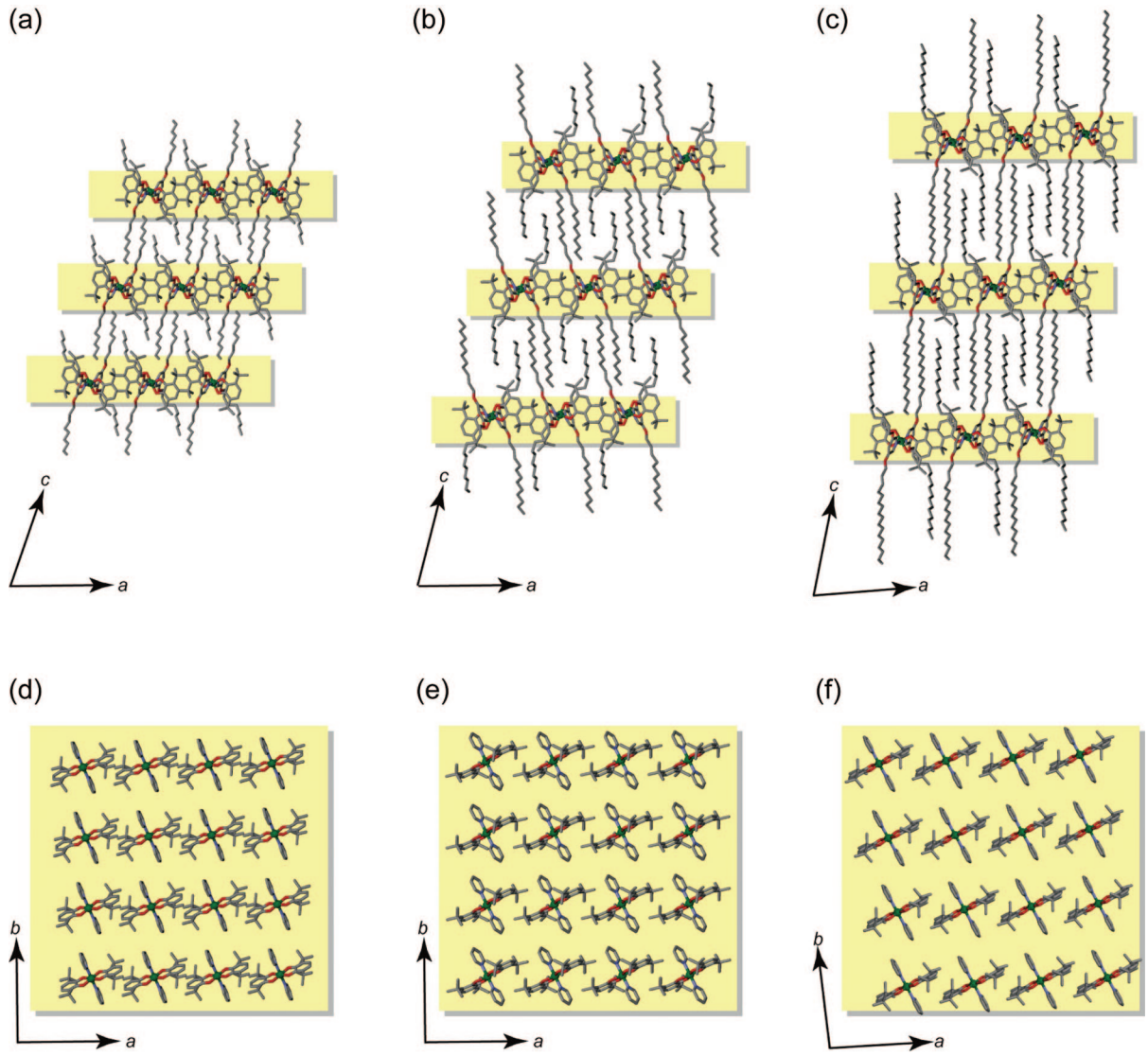

Figure 7. Projection of the layer-by-layer structures of the VT moieties in **CoC*n*Opy** along the *b*-axis ((a) $n = 9$, (b) 12, and (c) 17) and projection of whole assembled structures along the *c*-axis ((d) $n = 9$, (e) 12, and (f) 17; alkoxy chains are omitted). Color code: green (Co), red (O), blue (N), and grey (C). Hydrogen atoms are omitted for clarity.

$\Delta S_{VT(x)}$ refer to the enthalpy and entropy gains during the VT equilibrium in the *x* phase (*x* refers to the supercooled melt or the solution discussed below), and *R* is the gas constant. Because all **CoC*n*Opy** show the essentially same properties, hereafter thermal parameters of **CoC12Opy** is mainly discussed and those of **CoC9Opy** and **CoC17Opy** are shown in Table 2 and Figure 6a,c. The best fit for the supercooled melt of **CoC12Opy** gave $\chi T_{hs\text{-}[Co^{II}]} = 2.97$ cm^3 K mol^{-1}, $\Delta H_{VT(melt)} = 43.3$ kJ mol^{-1}, $\Delta S_{VT(melt)} = 137$ J mol^{-1} K^{-1}, and the equilibrium temperature, $T_{VT(melt)} = \Delta H_{VT(melt)}/\Delta S_{VT(melt)}$), $= 316$ K ($R = 0.9996$), using 0.55 cm^3 K mol^{-1} as the fixed $\chi T_{ls\text{-}[Co^{III}]}$ limit obtained at 200 K. In addition to the above results, the temperature-dependent $\chi_M T$ of a toluene solution including **CoC12Opy** was obtained by the Evans method[50] (Figure 6). The observed $\chi_M T$ values were fitted by eq 1 to give $\chi T_{hs\text{-}[Co^{II}]} = 2.45$ cm^3 K mol^{-1}, $\Delta H_{VT(solution)} = 46.5$ kJ mol^{-1}, $\Delta S_{VT(solution)} = 154$ J mol^{-1} K^{-1}, and equilibrium temperature, $T_{VT(solution)} = \Delta H_{VT(solution)}/\Delta S_{VT\text{-}(solution)}$, $= 302$ K ($R = 0.9998$), where the $\chi T_{ls\text{-}[Co^{III}]}$ limit was fixed to 0.53 cm^3 K mol^{-1} obtained at 203 K. Surprisingly, the observed T_m (367 K for **CoC12Opy** as in Table 2) is higher by 51 and 65 K than the equilibrium temperatures of the supercooled melt and in the solution ($T_{VT(melt)}$ and $T_{VT(solution)}$), respectively, demonstrating a strongly suppressed VT interconversion from the ls-[Co^{III}] to the hs-[Co^{II}] in the crystal lattice ($T_{VT(melt)}$, $T_{VT(solution)} < T_m$) and this is also the case for the **CoC9Opy** and **CoC17Opy** as shown in Table 3.

To understand the suppressed VT interconversion, it is quite instructive to look at the crystal structures of the ls-[Co^{III}] form. Here we noted that all the **CoC*n*Opy** commonly form layer-by-layer structures (Figure 7a−c) constructed from a two-dimensional layer of the central VT moieties sitting on the *ab*-plane (Figure 7d−f) and those of interdigitated alkoxy chains. These structures could result from efficient microsegregation of the nonpolar alkoxy chains and the polar ls-[Co^{III}] core toward the stabilization of the crystalline phases.[51,52] Although the absolute configuration of the intramolecular dipole moments

(50) Evans, D. F. *J. Chem. Soc.* **1959**, 2003–2005.

(51) Taga, T.; Miyasaka, T. *Acta Crystallogr.* **1987**, *C43*, 748–751.
(52) Fukunaga, H.; Takimoto, J.; Doi, M. *J. Chem. Phys.* **2004**, *120*, 7792–7800.

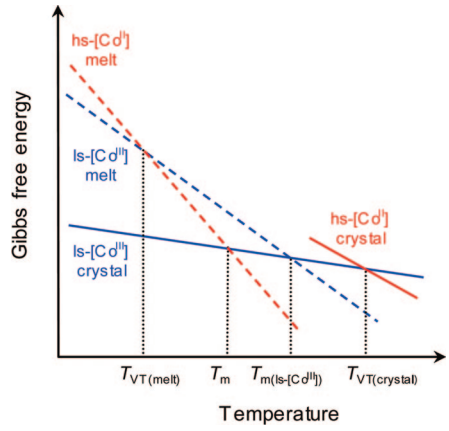

Figure 8. A Gibbs free energy versus temperature diagram for the synchronic bistability. $T_{VT(melt)}$ is the VT equilibrium temperature in isolated state (melt), T_m is the temperature of the synchronic bistabiltiy, $T_{m(ls\text{-}[Co^{III}])}$ is the melting temperature of ls-[Co^{III}] crystal, and $T_{VT(crystal)}$ is the VT equilibrium temperature in crystalline phase. $T_{VT(crystal)}$ could not be observed because of the melting (T_m) is at a lower temperature than $T_{VT(crystal)}$.

could not be decided because of the presence of the crystallographic inversion center on the Co atom, the synchronic bistability implies that the well-organized crystalline phase would only be stabilized by the mixed-valent, polar ls-[Co^{III}] form. That is to say, the ls-[Co^{III}] form is forced to maintain its charge distribution within the crystal lattice until the whole packing structure becomes thermally unstable. In fact, the ls-[Co^{III}] form is thermally altered to the homovalent, nonpolar hs-[Co^{II}] form accompanied by melting of the crystal at T_m.

We next consider the temperature at which the ls-[Co^{III}] crystal melts to form the corresponding liquid in the absence of the VT interconversion. From the additivity of the thermodynamic parameters of the crystal-melt phase transition and the VT interconversion represented in eqs 2 and 3, respectively, a supposed melting temperature of the ls-[Co^{III}] crystal, $T_{m(ls\text{-}[Co^{III}])}$, can be estimated from eqs 2−4:

$$\Delta H_{m(ls-[CoIII])} = \Delta H_m - \Delta H_{VT(melt)} \quad (2)$$

$$\Delta S_{m(ls-[Co^{III}])} = \Delta S_m - \Delta S_{VT(melt)} \quad (3)$$

$$T_{m(ls-[Co^{III}])} = \Delta H_{m(ls-[Co^{III}])}/\Delta S_{m(ls-[Co^{III}])} \quad (4)$$

where $\Delta H_{m(ls\text{-}[Co^{III}])}$ and $\Delta S_{m(ls\text{-}[Co^{III}])}$ are the enthalpy and entropy gains in the supposed crystal-to-melt phase transition of the ls-[Co^{III}] form. The important implication of the parameters obtained from these calculations is that the outward melting temperature of the ls-[Co^{III}] crystal of **CoC12Opy** is estimated to be 415 K, which is significantly higher by 48 K than T_m ($T_m < T_{m(ls\text{-}[Co^{III}])}$) and this is also the case for the corresponding **CoC9Opy** and **CoC17Opy** as shown in Table 3. That is, the synchronicity of the molecule-based VT interconversion and the macroscopic crystal-to-melt phase transition resulted in the significant acceleration of the macroscopic melting phenomenon.

Summarizing all these considerations, together with the analytically obtained sequence of $T_{VT(melt)}$, $T_{VT(solution)} < T_m < T_m$(ls-[$Co^{III}$]), the synchronic bistability can be simply represented in terms of the Gibbs free energy versus temperature ($G-T$) diagram shown in Figure 8, where $T_{VT(crystal)}$ refers to a supposed VT equilibrium temperature in the crystalline phases.[53] An important feature of the diagram for the synchronic bistability is that T_m is higher than $T_{VT(melt)}$ ($T_{VT(melt)} < T_m$). This relation implies the *enthalpically* stabilized ls-[Co^{III}] crystal phase with the microsegrated structure constructed from the mixed-valent ls-[Co^{III}] form and the well-ordered alkoxy chains. This negative *enthalpic effect* leads to a significant decrease of the Gibbs energy curve for the ls-[Co^{III}] crystal, thereby thermodynamically preventing the VT interconversion in the crystalline phase. Second, the doping of the alkoxy chains affects an increase of the Gibbs energy slope ($\Delta G = -S$) of the melts as a positive *entropic effect*,[54] leading to the appearance of T_m at a temperature lower than $T_{VT(crystal)}$. These two features strongly demonstrate that both *the enthalpic* and *the entropic effects* attributed to the alkoxy chains serve as thermodynamic driving forces of the unprecedented synchronic bistability.

4. Conclusion

In summary, the present results demonstrate a new strategy to achieve significant synchronicity of the molecule-based bistability derived from the VT interconversion with the macroscopic crystal-melt phase transition. Here emphasis is placed on first that we have succeeded in perfectly synchronizing molecule-based bistability triggered by a thermally induced intramolecular one-electron transfer process with a macroscopic phase transition from a three-dimensionally ordered solid to a perfectly disordered liquid. Second, we have shown the thermodynamic mechanism of the synchronic bistability and demonstrated that the doping of alkyl chains into a bistable molecular system is a quite powerful strategy to transcribe the molecular phenomena into the macroscopic events. These findings imply that the bistability at the molecular level should induce a drastic phase transformation sufficiently large to allow easy detection by a change in macroscopic properties. Finally, the promising aspects of the proposed regime are not restricted to a thermal event; there is a possibility of nonthermal melting and crystallization based on the photo and pressure-responsiveness of the VT interconversion.[37,38e,49]

Acknowledgment. We thank Prof. Kazuya Saito and Dr. Yasuhisa Yamamura in University of Tsukuba for helpful discussion on the thermal analysis. We also thank Prof. Cortlandt G. Pierpont in University of Colorado for his helpful discussion. This work was supported by a Grant-In-Aid for Science Research from the Ministry of Education, Culture, Sports, Science and Technology, Japan.

Supporting Information Available: Synthesis of [Co(3,6-DTBSQ)$_3$], the estimated scan rates for magnetic susceptibility measurements, temperature dependent magnetic susceptibility and DSC data on second heating process, and crystallographic data in CIF format. Movies for the melting and crystallization processes of **CoC12Opy**. This material is available free of charge via the Internet at http://pubs.acs.org.

JA711268U

(53) The $T_{VT(crystal)}$ could not be determined experimentally; however, this does not affect the discussion and the conclusion made in this manuscript.

(54) Sorai, M.; Saito, K. *The Chemical Record* **2003**, *3*, 29–39.